telecom

MDPI

Review

RIS-Assisted Covert Communication for Millimeter-Wave MIMO Channels in Railway Internet of Things

Zepeng Zhang [1,*], Man Yang [2] and Jiange Jiang [3]

[1] College of Electronic Engineering, Lanzhou City University, Lanzhou 730070, China
[2] College of Information Engineering, Lanzhou City University, Lanzhou 730070, China; yangman@lzcu.edu.cn
[3] College of Information Engineering, Jingdezhen Ceramic University, Jingdezhen 333403, China; m13340110704@163.com
* Correspondence: zhangzepeng@lzcu.edu.cn

Abstract

As the railway industry undergoes digital transformation driven by AI, big data, and 5G/6G, secure data transmission for IoT-oriented railway operations has become a critical challenge in high-speed railway (HSR) wireless communications. Covert communication, which conceals wireless transmissions from eavesdroppers, together with reconfigurable intelligent surfaces (RISs), MIMO, and millimeter-wave technologies, offers a promising solution for enhancing security in such dynamic environments. This paper presents a comprehensive review of RIS-assisted covert communication for mmWave MIMO channels in HSR IoT networks. We examine security threats and the limitations of existing schemes, introduce the system architecture and channel modeling approaches, and summarize Doppler shift compensation techniques for high-mobility scenarios. In particular, this review introduces a service-priority-based covert constraint design framework as an original analytical perspective, rather than a fully validated engineering solution, to improve adaptability in diverse HSR operational contexts. We further provide a critical comparative review of optimization algorithms, including convex relaxation, heuristic, and deep reinforcement learning approaches, with a focus on their applicability and complexity trade-offs, and outline future research directions. Beyond summarizing the existing literature, this review integrates new analytical perspectives and simulation-based illustrations derived from our recent publications, offering both a systematic reference and forward-looking insights for researchers in this emerging field.

Keywords: 6G communication systems; high-speed railway (HSR); internet of things (IoT); reconfigurable intelligent surface (RIS); wireless covert communication

Check for updates

Academic Editors: Triantafyllos Kanakis, Charan Litchfield and Achilles Boursianis

Received: 2 August 2026
Revised: 16 September 2026
Accepted: 4 October 2026
Published: 13 October 2026

Copyright: © 2026 by the authors. Licensee MDPI, Basel, Switzerland. This article is an open access article distributed under the terms and conditions of the Creative Commons Attribution (CC BY) license.

1. Introduction

1.1. Background

Information and communication technology is a crucial enabler of intelligent railways. In the fifth-generation (5G)-enabled intelligent HSR communication system, the scale of IoT devices and the volume of data transmission are expected to increase explosively [1,2]. However, to meet the needs of free movement of IoT terminals, the wireless networking mode and the broadcast nature of wireless channels make both 5G Railway (5G-R) and the upcoming 6G-R vulnerable to external signal interference and attacks [3–5]. For example, in the new generation of railway IoT driven by 5G, massive sensing equipment and mobile terminals will face potential risks of eavesdropping and attacks. The data generated by

railway IoT devices include confidential business data and user information, which, once leaked, will cause significant damage to the privacy of enterprises and users. Eavesdroppers may monitor the wireless channel to determine whether communication is taking place. As a result, the train scheduling data and the user's privacy data are being seriously threatened by illegal eavesdropping devices, with this threat intensifying as visions such as ubiquitous connectivity and twin cities are progressively implemented [6,7].

1.2. Related Work and Contribution

To ensure the safe transmission of data, cryptography-based upper layer encryption technology is widely used. However, with the advent of supercomputing technologies such as quantum computing, this mathematical encryption method could be cracked within a short period of time. In addition, side-channel attack techniques like timing attack, energy attack, and electromagnetic attack can avoid complex mathematical logic and directly extract the information. The overhead associated with the management and distribution of keys would likewise be prohibitive. If the identical password protocol is used, the risk of being decoded similarly escalates [8].

As a complement to encryption technology, physical layer security inherently prevents eavesdropping by exploiting channel randomness and variability [9,10]. However, secure communication encompasses not merely the prevention of eavesdropping on content; it is equally crucial to conceal communication behavior. Undetected communication behavior can mitigate eavesdropping or decryption. Wireless covert communication provides a solution for the concealment requirement of HSR communication systems because it can hide the communication behavior [6,7,11]. In the HSR communication scenarios, the eavesdropper typically uses a high-precision energy meter for detection. Therefore, how to ensure the signal quality of trains in the 5G-R network while realizing reliable covert communication and reducing the cost is the issue to be solved urgently.

Recently, the RIS technology has been widely used in the field of wireless communication [2,12–14]. RIS is a surface containing a large number of passive reflective elements, each of which can independently introduce controllable amplitude and phase shifts to the incident signals. By densely deploying RIS within a wireless communication system and finely tuning its parameters, it is possible to improve communication performance by increasing the expected power gain of the received signal and minimizing interference destructively. RIS naturally has the outstanding characteristics of low cost, low complexity, and easy deployment, which can solve the challenges in intelligent HSR communication scenarios well [15,16]. Combined RIS, MIMO, and millimeter-wave technology can reduce the Doppler shift and penetration loss of high-speed trains, expand the coverage of Base Stations (BSs), enhance the transmission power of the signal, and promote the global deployment of 5G-R networks [17,18]. In RIS-assisted railway IoT communication systems, hidden communication behavior is also of great significance, such as whether communication occurs, its timing characteristics, whether the carrier is the train or a passenger, the communication location, and the movement track of the Mobile Relay (MR). Therefore, this study focuses on the RIS-assisted covert communication for IoTs in the HSR environment.

It is worth noting that, in addition to RF/mmWave links, optical wireless and fiber-based communication technologies are also emerging as complementary solutions for railway communication networks, offering ultra-high bandwidth and low latency for future 5G/6G railway IoT systems [19]. Hybrid RF/optical architectures can leverage the strengths of both domains as follows: mmWave/RIS links provide flexible coverage and covert communication capabilities, while optical links deliver high-capacity backhaul and fronthaul connectivity. This complementary integration represents a promising direction for enhancing the overall resilience and capacity of railway communication networks.

The contributions of this manuscript are classified into the following four categories:

(1) Models and results reproduced or adapted from the prior literature: The basic covert communication model, the binary hypothesis-testing framework, the square-root law, and the fundamental system architecture in Figure 1 are adapted from foundational works such as Bash et al. [20], Wang et al. [21], and Chen et al. [11]. These are clearly cited and presented for self-containedness.

(2) New formulations introduced by the authors: The service-priority-based covert constraint design was originally proposed by our research team. This formulation extends the conventional KL-divergence-based covertness constraint by incorporating three-tiered HSR business priorities, which, to the best of our knowledge, has not been reported elsewhere. In addition, the comparative classification of Doppler compensation schemes with the recommendation of Scheme 3 for HSR scenarios reflects our original analytical perspective.

(3) New simulation results generated specifically for this manuscript: The numerical results presented in the comparison of Doppler shift compensation schemes, as well as in the relationship between covert throughput and the number of antennas under two asymmetric KL constraints, are newly generated for this review paper. These simulations are not directly reproduced from any single prior publication; rather, they are synthesized from our team's prior work [6] with updated parameters and serve to illustrate and support our comparative discussions.

(4) Content that is review, commentary, and comparative analysis: The comprehensive survey of covert communication-enabling techniques, the systematic categorization and complexity comparison of optimization algorithms, the performance–runtime trade-off analysis, and the entire discussion on future research directions constitute the core review content of this paper. These sections synthesize findings from over 100 references and provide critical comparisons and insights, rather than presenting new technical solutions.

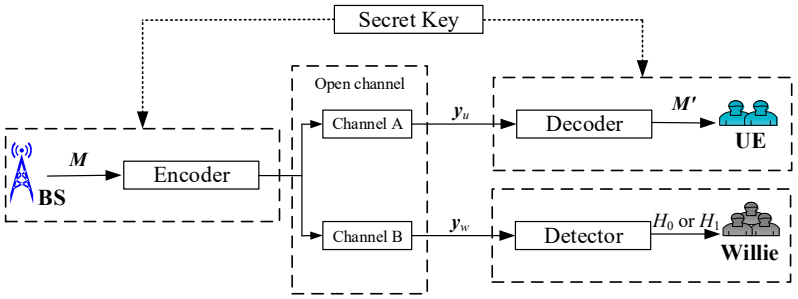


Figure 1. The typical wireless covert communication system model.

The rest of the paper is organized as follows. In Section 2, this review examines the basic concept of covert communication and related work. In Section 3, this review examines how to build a RIS-assisted millimeter-wave MIMO covert communication model in a railway IoT network, summarize the three Doppler shift compensation methods, and propose a covert constraint design method based on business priority. In Section 4, this review summarizes the existing algorithms for solving NP-hard problems with the example of maximizing covert throughput. In Section 5, we point out the future challenges of RIS-assisted MIMO covert communication research in HSR scenarios. Finally, we conclude this paper in Section 6.

Notations: The notations used in this paper are as follows. Let $\boldsymbol{a}$ and $\boldsymbol{A}$ denote a vector and a matrix, separately. $\boldsymbol{x}^{\mathrm{H}}$ and $\boldsymbol{X}^{\mathrm{H}}$ denote the conjugate transpose of a vector x or a matrix $\boldsymbol{X}$. $\mathbb{C}^{M\times N}$ stands for the set of $M \times N$ complex-valued matrices. $\mathcal{CN}$ $(0, \Sigma)$ represents the

distribution of a circularly symmetric complex Gaussian with zero mean and variance Σ. $\sim$ stands for "distributed as". $|\cdot|$ denotes the absolute value. The rank of $\boldsymbol{S}$ is denoted by rank ($\boldsymbol{S}$). The key symbols used throughout this paper, along with their descriptions and dimensions, are summarized in Table 1 for quick reference. It should be noted that, unless otherwise specified, the key parameter settings used in the simulation analysis in this article are uniformly as shown in Table 1. The other unlisted parameters can be referred to the cited references we provided.

Table 1. System model parameters and simulation parameter description.

Symbol	Description	Dimension/Domain	Symbol	Description	Dimension/Domain
$\boldsymbol{H}_{BR}$	Channel matrix of BS-RIS link	$N_R \times N_B$	$\boldsymbol{G}_{RW}$	Channel matrix of RIS-Willie link	$N_W \times N_R$
$\boldsymbol{G}_{BM}$	Channel matrix of BS-MR link	$N_M \times N_B$	$\boldsymbol{\Theta}$	RIS reflection coefficient matrix	$N_R \times N_R$
$\boldsymbol{H}_{RM}$	Channel matrix of RIS-MR link	$N_M \times N_R$	$\mathbf{w}_B$	BS transmit beamforming vector	$N_B \times 1$
$\boldsymbol{W}_{MW}$	Channel matrix of MR-Willie link	$N_W \times N_M$	$\mathbf{w}_M$	MR receive beamforming vector	$N_M \times 1$
$\boldsymbol{H}_{BW}$	Channel matrix of BS-Willie link	$N_W \times N_B$	N_B, N_M, N_W, N_R	Number of antennas/ elements at BS, MR, Willie, and RIS	8, 8, 8, 16
f_c	Carrier frequency	28 GHz	σ_M^2, σ_W^2	Noise power	-110 dBm
$\boldsymbol{B}$	System bandwidth	500 MHz	P_B	BS transmission power	42 dBm
v	Train velocity	250 km/h	K	Packet length	200
ε	Covertness threshold parameter	[0, 1]	d	Antenna element spacing	$\lambda/2$

The literature-search methodology: To ensure the comprehensiveness and reproducibility of this review, we conducted a systematic literature search using the following databases: IEEE Xplore, Web of Science, Scopus, and CNKI (China National Knowledge Infrastructure). The search covered the period from 2013 (when Bash et al. first formulated the covert communication capacity problem) to 2026. The primary search terms included combinations of: "covert communication," "low probability of detection," "physical layer security," "reconfigurable intelligent surface," "intelligent reflecting surface," "high-speed railway," "railway IoT," "millimeter-wave," "MIMO," "Doppler shift," "beamforming," and "finite block length."

The inclusion criteria were: (i) peer-reviewed journal articles and conference proceedings; (ii) works addressing covert communication theory, RIS-aided transmission, or HSR wireless communications; (iii) papers that provide analytical models, optimization frameworks, or performance evaluations relevant to the scope. We excluded non-English publications (except for a few key Chinese-language papers on HSR-specific topics) and works without explicit system models or quantitative results. The retrieved papers were initially screened by title and abstract, followed by full-text assessment. Finally, 115 papers were selected and categorized into thematic groups as follows: covert communication fundamentals (Section 2), RIS/HSR channel modeling (Section 3), and optimization algorithms (Section 4). This structured process ensures that our review is both systematic and reproducible.

2. Wireless Covert Communication Model

Bash et al. [20] first framed communication behavior detection as a binary hypothesis-testing problem, suggested analyzing covert communication capacity via information theory, and demonstrated the square-root law for covert capacity. However, subsequent research [21–23] revealed that positive covert capacity can be achieved in systems with numerous uncertainties, including noise, channel fading, interference, etc. In this section, we first introduce the basic model of covert communication and the commonly used covert performance indicators. Then, the approaches to achieving positive concealment capacity are summarized, considering noise uncertainty, channel uncertainty, interference, finite block length, etc. Notably, these methods may overlap.

2.1. Related Concepts of Wireless Covert Communication

As shown in Figure 1, the typical wireless covert communication system model includes BS, User Equipment (UE), and unauthorized eavesdroppers (Willie). The BS covertly transmits communication signals to the UE under the Willie's surveillance. Willie ascertains the communication status of the BS and UE based on power variations. Details of covert communication transmission can be found in reference [8].

Similar to existing works on covert communications, we assume that Willie performs the statistical hypothesis test to detect the existence of transmission from BS. In particular, the null hypothesis, H_0, represents that BS keeps silence, while the alternative hypothesis, H_1, indicates that BS is on for transmission. Under the two hypotheses mentioned above, the signal received by Willie is given as follows:

$$Y_W(i) = \begin{cases} I(i) + N(i), & H_0 \\ S(i) + I(i) + N(i), & H_1 \end{cases} \tag{1}$$

where i denotes the index of the signal symbol. Variables $I(i)$, $N(i)$, and $S(i)$ are the interference, noise, and signal received by Willie, respectively.

Following a common assumption adopted in existing works, we assume that the prior probabilities of hypotheses H_0 and H_1 are equal, i.e., $\pi_0 = \pi_1 = 0.5$, for simplicity. Note that this assumption can be directly extended to the case with arbitrary prior probabilities of hypotheses. Then, the detection error probability at Willie, ξ, is given by

$$\xi = \pi_0 \Pr(D_1 \mid H_0) + \pi_1 \Pr(D_0 \mid H_1) \tag{2}$$

where D_0 and D_1, respectively, denote the decision made by Willie in the favor of H_0 and H_1. Specifically, $0 \leq \xi \leq 1$. If $\xi = 0$, Willie can detect the signal transmission from BS perfectly. On the other hand, if $\xi = 1$, Willie cannot make a correct detection at the time, i.e., a blind guess.

Therefore, when constructing the optimization problem of covert communication, the lower bound of ξ is usually taken as the covert performance index, i.e.,

$$\xi \geq 1 - \varepsilon \tag{3}$$

where the term $1 - \varepsilon$ denotes the minimum required probability for Willie to make a wrong decision. The study of covert constraints is described in detail in Section 3.2.

2.2. Technologies Related to Covert Communication

In view of the capacity limit of the square root law proposed in the literature [20] and the possible technical scheme of realizing positive covert rate proposed in the literature [21–23], relevant teams have conducted a lot of research. Based on hypothesis-

testing theory and information theory, performance analysis and scheme optimization are carried out, which provided a solid theoretical basis for the practice of covert communication engineering. In general, the introduction of uncertainty enables higher-performance covert communication. The following four covert communication schemes have been widely used and studied.

Covert communication based on the uncertainty of noise. Taking advantage of Willie's lack of certainty about noise in the environment, noise uncertainty can be introduced to increase its detection error probability. The literature [21,24–28] and others explored the possibility of using noise generated by a transmitter, jammer, or relay to confuse Willie's judgment under different conditions. It is found that adding different power noises to the channel can achieve positive concealment rate and increasing the power of noise appropriately can improve the concealment performance of the system. In fact, in real communication scenarios, the uncertainty of noise cannot be avoided due to temperature changes, noise changes, and calibration accuracy. Therefore, it is of practical significance and necessity to study the scheme of using natural noise or artificial noise in the environment for covert communication.

Covert communication based on the uncertainty of the channel. The literature [29] revealed the possibility of BS using channel uncertainty to achieve positive rates. Based on the real-time Channel Status Information (CSI) and statistical CSI, the limits of the covert capacity under the constraint of relative entropy are derived, respectively. It is proved that the positive rate can be realized in some cases by relying on channel information. In addition, interference signals with random power generated by UE can also confuse Willie's detection [6,21]. However, this approach requires the UE to have the capability of self-interference cancelation (SIC). In addition, the randomness introduced by the power of the self-interfering signal may cause communication interruption at the UE. In general, wireless covert communication based on channel uncertainty must require a communication bunker so that this uncertainty can be converted into Willie's detection uncertainty.

Covert communication based on assisted interference. In practice, it is more difficult to hide the signal completely in the background noise. However, assisted interference can produce randomly varying interference power, increasing the probability of Willie's detection error. The literature [30] proved that under AWGN and quasi-static Rayleigh fading channels, extra jammers can bring positive rates. The literature does not require jammers to know when BS communicates. For AWGN channels, by designing jammers to transmit Gaussian signals of different power in the time slot where BS may communicate, the effect equivalent to the uncertain noise power is achieved. The study of the literature [31] provided a reference for the scheme design of medium- and long-distance wireless covert communication. Specifically, it introduced an amplified relay with the ability to assist interference and took the randomness of the relay transmitting interference power as a covert source to confuse Willie.

Covert communication based on finite block length. It is impractical to assume that Willie can use an infinite number of samples for covert communication with binary detection, especially in some cases where the number of channel uses is limited or in ultra-reliable low-latency scenarios [32]. This is because infinite block-length communication makes Willie more capable of detecting the transmission. The literature [23] studied the game problem between transmission reliability and concealment for short-packet covert communication scenarios. In [33], considering the influence of pilot leakage on covert communication over finite block length, a multi-antenna joint covert communication model is constructed. The hidden throughput maximization problem subject to hidden constraints, transmission reliability, and block length constraints is established, and a simple and reliable solution is proposed. The literature [34] has developed a reliable scheme for covert

transmission on multi-carrier channels with limited power and a limited block length budget. At present, the problem of whether the finite block length and infinite block length covert communication schemes are compatible in the same scenario still needs to be further explored. In addition to the above, a small number of studies have also proposed the use of transmission time uncertainty [35], multi-node covert network [36], path loss model [37], multi-hop relay [38], multi-antenna emission [39], and other schemes to achieve positive covert capacity.

Recently, some research has begun to explore the integration of traditional covert schemes with emerging technologies such as RIS and Unmanned Aerial Vehicles (UAVs). For example, Wang et al. [21] studied RIS-assisted covert communication. It is proved that RIS can change the phase shift in the signal and improve the covert transmission rate of the systems. The literature [6] studied the covert throughput maximization of RIS-assisted HSR communication systems. To achieve reliable covert communication, the authors assumed that the receiver generated a jamming signal of varying power to confuse Willie. Considering the Doppler shift in the train and finite block length, an alternate optimization algorithm is proposed to design the active and passive beamforming of BS and MR. Simulation results verified the effectiveness of the proposed algorithm. In addition, the literature [22] et al. studied covert communication involving UAVs from different angles. However, the flight range and distance of UAVs may affect the safety of trains [40], so the integration of low-altitude economy and rail transportation field needs to be further studied.

The covert communication techniques that can achieve positive covert rates in HSR communication systems are summarized in Table 2. It should be noted that in actual networks, these methods are not mutually exclusive and they can work together to improve the concealment of wireless communication networks.

Table 2. Existing covert communication techniques.

Techniques	Refs.
Noise uncertainty	[21,24–27]
Channel uncertainty	[6,21,29,41,42]
Time uncertainty	[35]
Location information uncertainty	[2,43–45]
Finite block length	[23,33,34,46]
Multi-node covert network	[36,47]
Path loss model	[37–43]
Multi-antenna emission	[27,48–52]
Multi-hop relay	[38]
RIS	[2,6,7,52]

3. RIS-Assisted MIMO Covert Communication System for HSR

In this section, this review summarizes the typical model of wireless covert communication in HSR scenarios, analyzes the characteristics of fast time-varying channels, addresses the Doppler shift compensation problem, and proposes a new covert constraint design scheme based on the priority of HSR IoT communication services. It should be noted that the system model presented in this section is intended to provide a general architectural framework for RIS-assisted covert communication in HSR scenarios, synthesizing modeling approaches from the existing literature [5,6,21,53–55]. Its purpose is to establish a common reference point for the subsequent discussions on Doppler compensation, covert constraint design, and optimization algorithms, rather than to serve as a fully specified system model for a novel algorithmic contribution. Detailed derivations of specific modeling assumptions—including warden location uncertainty, jamming power

distribution, residual self-interference, and imperfect CSI models—can be found in the cited references [6,21,54,55].

3.1. Covert Communication Model of HSR

The RIS-assisted HSR covert communication model mainly consists of five parts, as shown in Figure 2. There are mainly high-speed moving trains, a multi-antenna BS deployed alongside the track, an RIS deployed between adjacent BS, multi-antenna eavesdroppers present in the environment, and trackside buildings that sometimes block the signal transmission. The function of RIS is to assist covert communication between the BS and the train, avoid obstacles, and alleviate signal deviation caused by the Doppler effect. In order to reduce penetration losses, it is usually assumed that the top of the train is equipped with a multi-antenna MR, which is used to communicate with the ground BS instead of the train and all the IoT devices inside the train [5,53]. Due to the high attenuation of millimeter-waves and the harsh propagation environment, we consider only the single reflection of the RIS.

Based on the above analysis, the received signal at MR is given by

$$\boldsymbol{Y}_M[i] = \boldsymbol{M}[i]\left(\boldsymbol{G}_{BM}[i] + \boldsymbol{H}_{RM}^H[i]\boldsymbol{\Theta}\boldsymbol{H}_{BR}[i]\right)\boldsymbol{F}^H[i]s_B[i] + \boldsymbol{N}_M[i] \tag{4}$$

where $\boldsymbol{M} \in \mathbb{C}^{N_M \times 1}$ and $\boldsymbol{F} \in \mathbb{C}^{N_B \times 1}$ represent the beamforming vector at the BS and at the MR; variable $\boldsymbol{G}_{BM} \in \mathbb{C}^{N_M \times N_B}$, $\boldsymbol{H}_{BR} \in \mathbb{C}^{N_R \times N_B}$, and $\boldsymbol{H}_{RM} \in \mathbb{C}^{N_M \times N_R}$ represent the channel matrix of BS-MR, BS-RIS, and RIS-MR links, respectively. Furthermore, $\boldsymbol{\Theta} \in \mathbb{C}^{N_R \times N_R}$ is the reflection coefficient matrix of RIS, $s_B[t] \sim \mathcal{CN}(0,1)$ is the covert information signal transmitted from BS, and $\boldsymbol{N}_M \sim \mathcal{CN}\left(0, \sigma_M^2\right)$ is the noise received at MR.

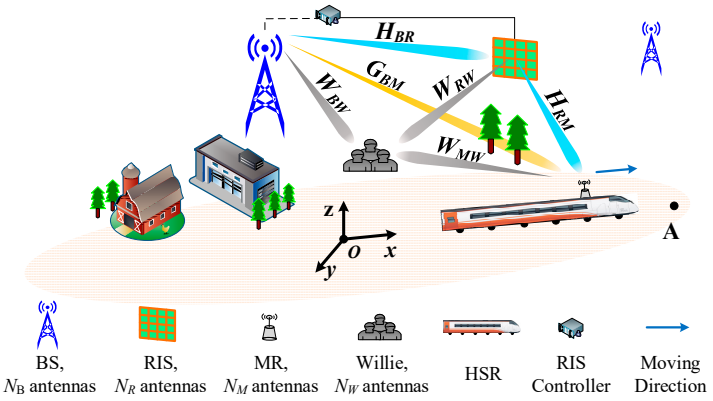


Figure 2. The RIS-assisted millimeter-wave MIMO covert communication model in HSR IoT network.

3.2. Wireless Channel Model and the Compensation of Doppler Shift

Considering the universality of the model, it is generally assumed that RIS is deployed in an ideal location with line-of-sight (LOS) components, and the Willie can be adaptively adjusted to a hidden location conducive to detection [54].

(1) Wireless channel model

In Figure 2, the positions of the BS, RIS, and Willie are fixed, but MR moves with the train. Therefore, we consider HBR, $\boldsymbol{W}_{BW} \in \mathbb{C}^{N_W \times N_B}$ (the channel between BS and Willie), and $\boldsymbol{W}_{RW} \in \mathbb{C}^{N_W \times N_R}$ (the channel between RIS and Willie) to be quasi-static millimeter-wave channels without Doppler shift. Variable $\boldsymbol{G}_{\mathrm{BM}}$, $\boldsymbol{H}_{RM}$, and $\boldsymbol{W}_{MW} \in \mathbb{C}^{N_W \times N_M}$ (the channel between MR and Willie) are time-varying millimeter-wave channels with Doppler shift.

With reference to the Saleh–Valenzuela model of millimeter-wave channel [54], the quasi-static channel HBR is modeled by

$$\boldsymbol{H}_{BR} = \sqrt{\frac{N_B N_R}{L_{BR}}} \sum_{\rho=1}^{L_{BR}} \alpha_\rho \boldsymbol{a}_r\left(\varphi_a^\rho, \theta_a^\rho\right) \boldsymbol{a}_t^H\left(\varphi_d^\rho, \theta_d^\rho\right) \tag{5}$$

where L_{BR} is the number of paths, and α_ρ is the channel coefficient of the ρ-th path. Variables $\boldsymbol{a}_r(\varphi, \theta)$ and $\boldsymbol{a}_t(\varphi, \theta)$ are the array response vectors of the BS and RIS, respectively. $\boldsymbol{a}^H$ represents the conjugate transpose of vector $\boldsymbol{a}$. Parameters φ_a, θ_a, φ_d, and θ_d are the signal arrival and departure azimuth and pitch angle of the BS-RIS link, respectively. For simplicity, we omit the signal symbol index i in the following, but the angle information needed for channel modeling is still associated with the position of MR in each symbol cycle. Research on train position and angle information can be obtained from [55].

(2) The compensation of Doppler shift

In scenarios where users move at slow speeds, the Doppler frequency shift between high-speed trains and the BS or RIS can significantly affect system performance [56–58]. To facilitate a clear comparison, the three Doppler shift compensation schemes considered in this review are uniformly referred to as Scheme 1, Scheme 2, and Scheme 3, respectively. Their definitions and modeling bases are summarized as follows.

Scheme 1 (Direct Incorporation): In this scheme, the Doppler shift is directly incorporated into the channel model as a random variable, and no on-demand compensation is performed. This approach follows the works in [59–61]. Scheme 2 (RIS-Assisted Compensation): In this scheme, the RIS phase shifts are designed based on prior train information, such as speed, position, and trajectory, to simultaneously maximize the instantaneous SNR and minimize the Doppler shift. This approach follows [18,19,62].

Scheme 3 (Outdated-CSI-Based Compensation): In this scheme, the relationship between the outdated CSI and the real-time CSI is modeled using the Clarke–Jakes spectrum with a temporal correlation coefficient. This approach follows [7,52,63,64]. Specifically, let Ts denote the delay between the outdated CSI and the real-time CSI. The relation between the outdated CSI $\widetilde{\boldsymbol{H}}[t]$ and the real-time CSI $\boldsymbol{H}$[t + Ts] is expressed as

$$\boldsymbol{H}[t + Ts] = \kappa \widetilde{\boldsymbol{H}}[t] + \sqrt{1 - \kappa^2} \Delta \boldsymbol{H}[t + Ts] \tag{6}$$

where $\kappa = J_0(2\pi\, f_D\, T_S)$ represents the temporal correlation coefficient or is termed as outdated CSI coefficient, f_D is the Doppler shift, $J_0(\cdot)$ is the zeroth-order Bessel function of the first kind, and $\Delta \boldsymbol{H}$ stands for the error term.

The performance of the three Doppler shift compensation schemes is compared in Figure 3 and Table 3. We assume that the speed of the train is 360 km/h and the center frequency of the system is 28 GHz. It can be seen that scheme 2 and scheme 3 have similar performance in compensating Doppler shift, both of which are better than scheme 1. As the train moves away from BS, the compensation capabilities of both schemes become more apparent. In addition, scheme 2 is slightly better than scheme 3, because RIS can accurately beamform the train at each location and compensate for frequency deviation. However, as previously analyzed, the computational complexity of scheme 2 is higher than that of scheme 3. Therefore, the selection of the Doppler shift compensation scheme should be suitable for practical application scenarios.

Table 3. Comparison of the three Doppler compensation schemes.

Aspect	Scheme 1	Scheme 2	Scheme 3
Required CSI	Statistical CSI only	Real-time CSI, train prior information (speed, position, trajectory)	Outdated CSI + temporal correlation coefficient
Computational Complexity	Low	High (requires per-location RIS phase shift optimization)	Medium
Update Frequency	Low (based on statistical distribution)	High (real-time per-symbol/location update)	Medium (depends on CSI update interval)
Robustness to Positioning Error	High (not sensitive to positioning)	Low (performance degrades with positioning inaccuracy)	Medium (depends on accuracy of correlation model)
Practical Implementation Requirements	Simple; no additional hardware needed	Requires RIS panel partitioning and real-time control; high hardware/software overhead	Requires historical CSI storage and delay estimation; moderate overhead
Applicable Scenarios	Low-speed or delay-tolerant scenarios	Scenarios with strict delay requirements and sufficient computational resources	High-speed scenarios with limited real-time CSI availability

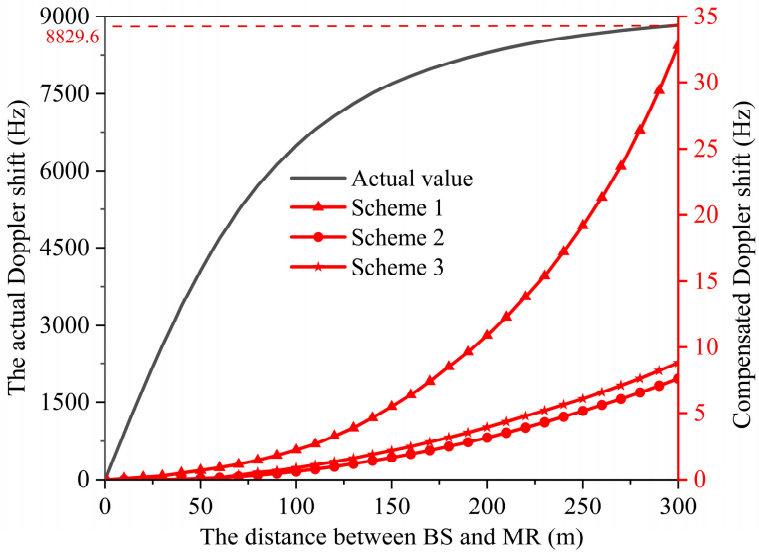


Figure 3. Performance comparison of three Doppler shift compensation schemes.

Given the rapid time-varying nature of the HSR wireless channel, it can be seen from the specific data in Figure 3 that the maximum Doppler shift in MR is 8829.6 Hz, and the coherence time obtained by calculation is about 113 μs, which is far less than the standard time slot length of 5G. Therefore, based on the main research content of this paper, we believe that scheme 3 is more suitable for HSR scenarios. If the influence of MR Mobility on time-varying channels is temporarily ignored, the modeling of time-varying channels $\boldsymbol{G}_{BM}$, $\boldsymbol{H}_{RM}$, and $\boldsymbol{W}_{MW}$ can be obtained by combining Formulas (4)–(6) with a smaller estimation error. In low-speed scenarios where delay requirements are low and high-priority services are not required, scheme 2 can also be used to compensate for the Doppler shift.

(3) Covert constraint design based on service priority

Based on the above-mentioned in Section 2.1, most existing studies use Kullback-Leibler (KL) diversity and total variation (TV) distance to improve the Willie's detection error probability and take it as a covert constraint [6,65,66]. The optimization goals usually aim to maximize covert transmission rate [21,65], channel capacity [7,67], or covert throughput [6,23,66], and so on. However, in HSR scenarios, to avoid system disorder, priority must be set for both the scheduling of IoT services and resource allocation. The system allocates parameters and performs corresponding actions based on business priority. Therefore, in the face of covert communication in HSR scenarios, it is necessary to set a high covert constraint level for higher-priority services to prevent important communication content from being eavesdropped. Considering the safety requirements and real-time performance of HSR services, we divide the main services into three levels and identify them with corresponding numerical quantification [68,69], as shown in Table 4.

Table 4. Priority classification of HSR communication services.

Priority Level	Representative Services	Numerical Value
High	Railway emergency calls, emergency voice/video communications, traffic-related scheduling communications, etc.	3
Medium	Non-vehicle-related scheduling communication, operation and maintenance voice/video communication, etc.	2
Low	Ordinary data communication/file transfer for users in the train, etc.	1

The priorities of HSR communications services are defined as follows: services that require high security levels and immediate response (milliseconds or even shorter) are defined as high priority. From the generation of services to the transmission there is a certain easing time (response time is obviously longer than the high-priority services), and the security levels are not strongly required to be defined as the medium priority. Common short-data communications/file transfers of users and low-security services that do not require response actions are defined as low priority. It should be noted that the priorities of medium and low services can be upgraded as appropriate.

To obtain a more tractable and analytically convenient covertness constraint, the original constraint (3) can be reformulated using the likelihood functions, KL divergence, total variation (TV) distance, and Pinsker's inequality. Specifically, let L_0 and L_1 denote the likelihood functions of Willie's observations under hypotheses H_0 and H_1, respectively. The total variation distance between the two distributions satisfies Pinsker's inequality:

$$T_V(L_x, L_y) \leq \sqrt{\frac{1}{2} D(L_x \| L_y)} \tag{7}$$

where $T_V(L_x, L_y)$ represents the TV distance between variables L_x and L_y, and $D(L_x||L_y)$ represents the KL diversity between variables L_x and L_y, $(x, y) = (0,1)$ or $(1,0)$. It can be seen that $D(L_x||L_y) \leq 2\varepsilon^2$ is more stringent than (3) [6]. This reformulated constraint (7) is a sufficient condition for (3), meaning that any system satisfying (7) automatically satisfies the original covertness requirement with a conservative safety margin. It is important to note that (7) is stricter than (3) and thus represents a more conservative design approach, which may reduce the achievable covert throughput but ensures more robust covertness performance.

Due to the asymmetry of relative entropy, the results obtained by using $D(L_0||L_1)$ and $D(L_1||L_0)$ as covert constraints are generally different [70]. In Figure 4a, assuming other variables remain unchanged, we compare the changes in system covert throughput

under two KL diversity conditions. We can see that the throughput under the two covert constraints increases with the number of BS's antennas. However, the covert throughput under the constraint $D(L_0||L_1) \leq 2\varepsilon^2$ is always higher than $D(L_1||L_0) \leq 2\varepsilon^2$. This is because $D(L_1||L_0) \leq 2\varepsilon^2$ is stricter than $D(L_0||L_1) \leq 2\varepsilon^2$, and this conclusion can also be found in [71].

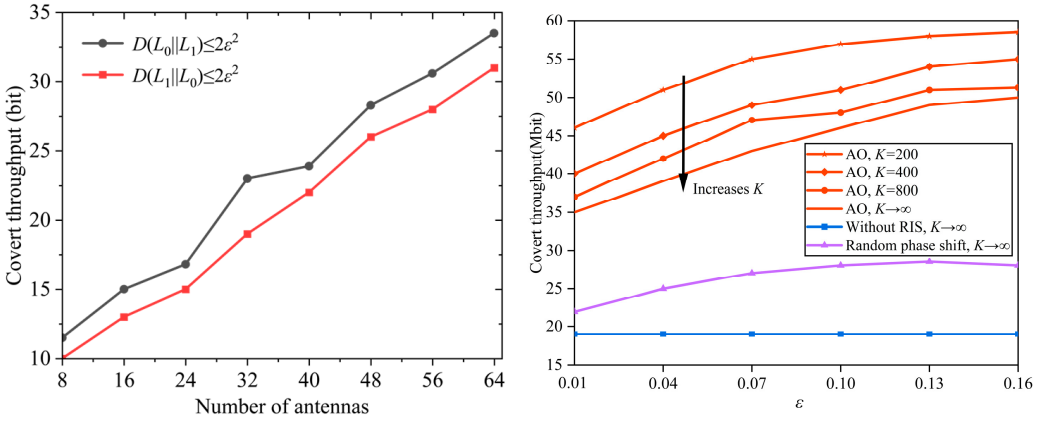


Figure 4. An example of the strictness analysis of covertness constraint parameters. (**a**) The asymmetry of relative entropy's influence on covert throughput; (**b**) The influence of covert constraint parameters on covert throughput.

The hidden constraint parameter x is strictly correlated with the priority of the business. We define that when ε is less than 0.04, it corresponds to high-priority business. ε falls within the range of 0.04 to 0.10 and corresponds to the most prioritized business of the medium category. For the lower-priority services, the value of ε is greater than 0.10. As shown in Figure 4b, as the priority of the service increases (ε decreases), covert throughput becomes smaller. This is because higher-priority covert services require a smaller ε to ensure secure transmission. A smaller x leads to a decrease in covert throughput. Furthermore, the figure also shows the impact of the data packet length K on the system. We set K to be 200, 400, and 800 respectively, corresponding to high-priority, medium-priority, and low-priority services. For high-priority services, the number of packets transmitted at one time should not be excessive; otherwise, the transmission becomes more vulnerable to eavesdropping. For more advanced operations, the number of packets should not be excessive; otherwise, it would be vulnerable to eavesdropping. Therefore, the smaller the value of K is, the fewer samples Willie can observe, and covert throughput will increase instead.

To sum up, in the HSR covert communication system, the design of covert constraints can be given by referring to Table 2 and equation $D(L_x||L_y) \leq 2\varepsilon^2$, where the values of (x, y) and ε are related to the priority of IoT services.

4. Optimization Algorithm for Covert Throughput

Based on the covert constraints, covert communication technologies, and the HSR covert communication model introduced in Sections 2 and 3, the RIS phase shift, BS transmit beamforming, and MR receive beamforming can be jointly optimized to achieve the desired goals, such as maximizing covert throughput (covert transmission rate), energy efficiency, and minimizing signal transmission delay. In this section, we will start from the construction of target problems and introduce and summarize the optimization algorithms to solve such problems.

4.1. Problem Formulation

Considering the system model shown in Figure 2, for covering the transmission from BS to MR, MR transmits jamming signals with varying power to confuse Willie on the detection of the covert communication. MR's self-interference channel, $f_M \sim \mathcal{CN}(0,\phi)$, where the SIC coefficient $\phi \in [0, 1]$ is determined by the efficiency of performing the SIC at MR. Considering short-packet communication of finite block length, the covert throughput at MR is given by

$$\eta = KR(1 - \delta) \tag{8}$$

where δ is the decoding error probability at MR, K is the packet length, and R is the information transmission rate from BS to MR, which is given by [72]

$$R = \log_2(1 + \gamma_M) + \sqrt{\frac{1}{K}\left(1 - \frac{1}{(\gamma_M + 1)^2}\right)}\frac{Q^{-1}(\delta)}{\ln(2)} \tag{9}$$

where $Q^{-1}(\cdot)$ represents the inverse Q function and γ_M is the Signal to Interference plus Noise Ratio (SINR) at MR, which is given by

$$\gamma_M = \frac{\left|\boldsymbol{M}\left(\boldsymbol{G}_{BM} + \boldsymbol{H}_{RM}^H \boldsymbol{\Theta} \boldsymbol{H}_{BR}\right)\boldsymbol{F}^H\right|^2}{\phi P_{Mi} + \sigma_M^2} \tag{10}$$

where P_{Mi} is the transmitting power of MR's interference signal.

When the packet length K and the decoding error probability δ at MR are determined, it is obvious that maximizing the system covert throughput is maximizing the SINR at MR. Therefore, the covert throughput maximization problem is formulated as

$$\begin{aligned} \max_{M,F,\Theta} \quad & \gamma_M \\ \text{s.t.} \quad & \text{C1: } D(L_1 \| L_0) \leq 2\varepsilon^2, \\ & \text{C2: } \|\boldsymbol{F}\|_2^2 \leq P_B, \\ & \text{C3: } |\boldsymbol{\Theta}_{m,n}| = 1, \\ & \quad m = 1, \cdots, N_{Rv}, n = 1, \cdots, N_{Rh}. \end{aligned} \tag{11}$$

where N_{Rv} and N_{Rh} are the number of rows and columns of RIS elements, respectively. C1 is the covertness constraint; the constraint C2 indicates the maximum BS transmission power limited to P_B; and the constraint C3 is the phase shift in RIS elements. Note that we use $D(L_1 \| L_0)$ as a covert constraint in this paper because we have already shown that $D(L_1 \| L_0)$ is greater than $D(L_0 \| L_1)$.

4.2. Optimization Algorithms

The primary challenges in achieving the optimal solution for problem (11) encompass the following. First, due to the constraints of the RIS unit module, the optimization problem is non-convex or NP-hard. Second, RIS phase shift, BS transmitting beamforming, and MR receiving beamforming in (10) are coupled to each other. Therefore, it is difficult to obtain the global optimal solution for this kind of problem. Most of the existing work focuses on obtaining efficient local optimal solutions with lower complexity, and some studies have confirmed that suboptimal solutions can also obtain better system performance than without RIS assistance.

Once the RIS phase shift is determined, the optimization problem transforms into a well-researched traditional beamforming design problem. Alternate optimization (AO) algorithms are usually used to decouple optimization variables. If the expression of SINR is more complex, the original problem can be transformed into a new manageable but

approximate problem using such things as the Weighted Minimum Mean Square Error (WMMSE) algorithm [73] or Fractional Programming (FP) [74]. This section will introduce and analyze the existing optimization methods, some of which have crossover, can be used alone, or can be used in combination under certain conditions.

(1) Traditional Algorithms

(a) Relaxation Algorithms (taking the Semidefinite Relaxation (SDR) as an example)

The SDR [75–81] method is the most common method for optimizing the phase shifts under constraint C3, i.e., for continuous phase shifts. Define $\boldsymbol{V} = \boldsymbol{\Theta}\boldsymbol{\Theta}^{\mathrm{H}}$. Then, the unit module constraint of RIS can be equivalent to $\boldsymbol{V} > 0$ and $\mathrm{rank}(\boldsymbol{V}) = 1$. By using the SDR method to remove the non-convex rank one constraint, the original problem is transformed into a convex semidefinite programming problem, which can be solved by CVX [81]. In general, the obtained relaxed problem is not a rank-one solution, i.e., $\mathrm{rank}(\boldsymbol{V}) \neq 1$. In this case, the Gaussian randomization method [6,61] is utilized to obtain a rank-one solution. Similar algorithms include Rank One Equivalents (ROEs) [82,83], relaxation and projection (RP) [84,85], etc.

(b) Manifold Algorithms (taking the Complex Circle Manifold (CCM) [86–88] as an example)

The constraint space in C3 can be regarded as the product of N_R complex circles. The original unit module constraint is transferred to the manifold space by projection, and the RIS phase shift is optimized by the gradient ascending or descending method to minimize the objective function. Finally, the optimal solution is obtained. However, before this, other constraints need to be eliminated by means of singular value decomposition, AO, or water-filling algorithm [55]. The challenge of manifold optimization algorithms resides in designing the gradient search direction and convergence conditions appropriately. Similar algorithms include Riemannian Manifold (RM) [55,89], etc.

(c) Gradient Algorithms (taking the Gradient Descent (GD) [90,91] as an example)

When the objective function $\gamma_{\mathrm{M}}(\boldsymbol{\Theta})$ is differentiable, the optimization problem can be solved by the GD method. Specifically, let $\boldsymbol{\Theta}^t$ be the phase shift vector at the t-th iteration. Then, the optimization variable $\boldsymbol{\Theta}$ at the $(t+1)$-th iteration is updated as

$$\boldsymbol{\Theta}^{t+1} = \exp\left(j\arg\left(\boldsymbol{\Theta}^t - \mu\nabla_{\boldsymbol{\Theta}}\gamma_M(\boldsymbol{\Theta})|_{\boldsymbol{\Theta}=\boldsymbol{\Theta}^t}\right)\right) \tag{12}$$

where μ is the step size, ∇_{Θ} is the gradient operator, and the $\arg(\cdot)$ operator is used for satisfying the unit-modulus constraint. The objective function can be maximized or minimized through a suitable design of the step size and gradient operator, iteratively optimizing the RIS phase shift. Other similar algorithms include Gradient Boosting (GB) [92] and Accelerated Projected Gradient (APG) [93,94], etc.

(d) Penalized Algorithms (taking the Penalty Convex-Concave Procedure (PCCP) [95–97] as an example)

The PCCP method equivalently rewrites the RIS unit module constraints and then uses the successive convex approximation method to transform the original non-convex constraints into a series of tractable approximate convex constraints. If necessary, it needs to define auxiliary variables to solve the RIS phase shift, and sometimes it also needs to solve the RIS phase shift by CVX. Similar algorithms include the Alternating Direction Method of Multipliers (ADMM) [75,98,99], the Barrier Function Penalty (BFP) [100,101], etc.

(e) Iterative Algorithms

The Block Coordinate Descent (BCD) [102–104] and the Majorization-Minimization (MM) [16,90,105] are two widely used iterative optimization techniques for RIS phase shifts. The difference is that the main idea of the BCD is to keep the reflection coefficients of other RIS elements unchanged and continuously optimize the phase shift in a single RIS

element in an iteration cycle until all phase shifts are optimized one by one. However, the MM algorithm is to approximate a complex problem into a series of more tractable subproblems, which are then solved iteratively. The MM algorithm needs to construct a surrogate function to replace the original objective function under specific conditions until the iterative process converges. Similar algorithms include the Block Coordinate Ascent (BCA) [106,107].

Traditional optimization algorithms mostly deal with non-convex and coupled problems through mathematical means, which is the basic method to solve NP-hard problems. However, such methods rely on assumed mathematical models, and the performance loss is sometimes not accurately characterized. With the increase in the number of antennas in the system, the algorithm complexity will be higher, and its application to the HSR fast time-varying scene remains to be studied.

(2) Heuristic Algorithms

Heuristic algorithms [108–110] are widely used in the field of non-convex optimization when the objective function is complex or the calculation of the gradient cannot converge for a long time. Taking Genetic Algorithm (GA) [108] as an example, we can regard the RIS phase shift as the chromosome of the individual in the population and the SINR as the fitness of each individual. Through iterative optimization, the individuals with low fitness are continuously eliminated, and the parents are generated in the remaining individuals with high fitness. After crossover, the offspring are generated for continuous evolution, and the final output of the chromosome with the highest fitness in the current population is the optimal RIS phase shift. Similar algorithms include Particle Swarm Optimization (PSO) [109,110].

The heuristic algorithm is suitable for solving combinatorial optimization problems because it has strong global search ability and can search for the global optimal solution with high probability. However, sometimes the convergence speed of the heuristic algorithm is slow, and the algorithm performance is more dependent on the parameter settings.

(3) Deep Reinforcement Learning (DRL) Algorithms

Model-free reinforcement learning (RL) is a dynamic programming tool that can be adopted to solve the decision-making problem by learning the optimal solution in dynamic environments. [111] For fast-moving scenarios, the literature [53,112–114] et al. began to study the use of RL methods to solve and optimize the RIS phase shift. Unlike supervised learning methods, the DRL methods do not require training labels, and the training phase with high complexity can also be optionally executed offline. Taking the Deep Deterministic Policy Gradient (DDPG) algorithm as an example [114,115], the RIS-assisted covert communication system (shown in Figure 2) can be regarded as an environment, and the central controller of the BS can be regarded as an agent. Problem (11) can be transformed into a Markov Decision Process (MDP) problem, where the state space is composed of the channel information, covert transmission rate, and covert constraint in a symbol period, i.e., $s_t = \left[\boldsymbol{G}_{BM}^{(t)}, \boldsymbol{H}_{BR}^{(t)}, \boldsymbol{H}_{RM}^{(t)}, R, \varepsilon\right]$. The action space consists of BS transmit beamforming, MR receive beamforming, and RIS phase shift, i.e., $\boldsymbol{a}_t = [\boldsymbol{M}^{(t)}, \boldsymbol{F}^{(t)}, \boldsymbol{\Theta}^{(t)}]$. The design of the reward function is related to the objective function and constraints. By appropriately designing the parameters of the neural network, a DRL framework with fast convergence and strong reliability can be trained to solve the RIS phase shift, as shown in Figure 5. During the network training process, the framework can also continuously acquire information from the environment and improve. The details of the DDPG algorithm can be found in [114,115]. Other similar algorithms include Convolutional Neural Networks (CNNs) [115], Deep Q-Learning (DQL) [112], and their derived algorithms [111].

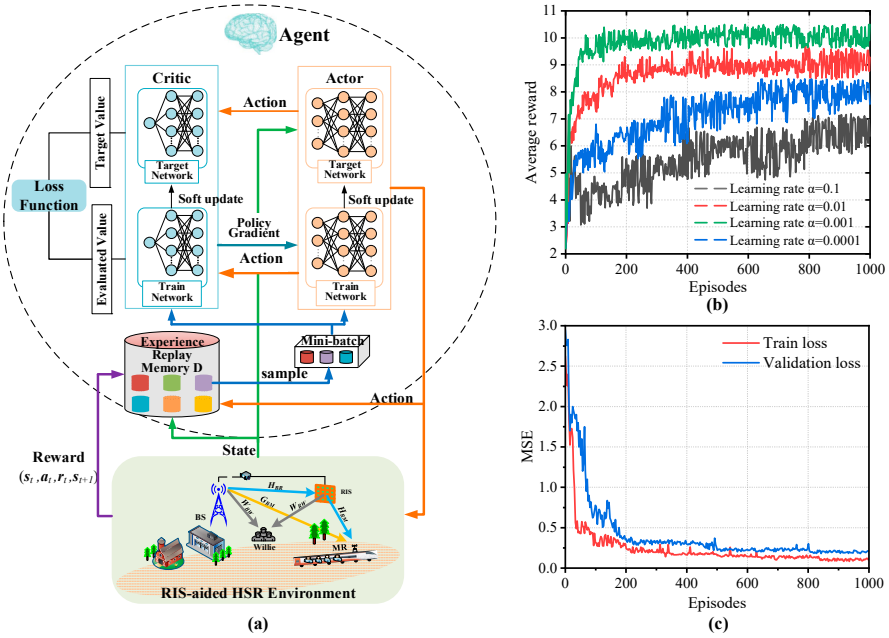


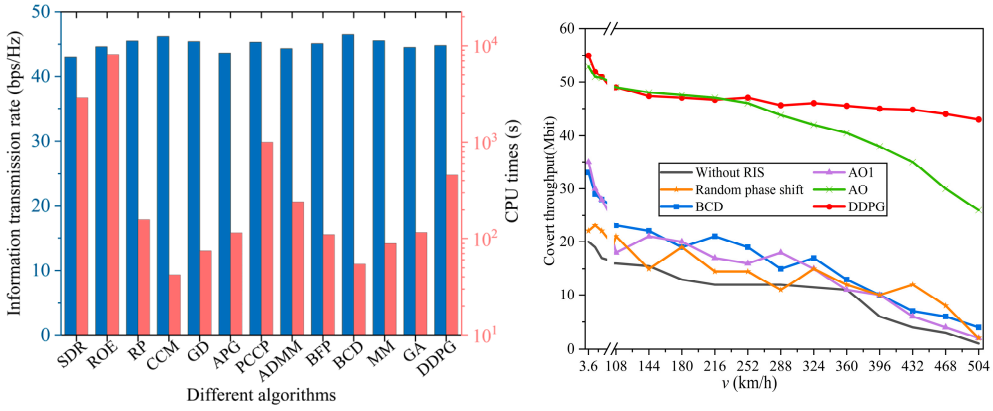
Figure 5. The DDPG framework used to solve Equation (11) and its performance. where (**a**) represents the DDPG framework; (**b**) To study the influence of the learning factor on the performance (average reward) of the DDPG neural network; (**c**) Comparison of training loss and validation loss for the DDPG neural network.

4.3. Complexity Analysis

In Table 5, we summarize the algorithms proposed in Section 4.2 and compare the highest order of magnitude (rather than the specific value) of computational complexity of each algorithm when solving the established non-convex problem. This is because these algorithms usually have different application scenarios and system models, and most of them need to be combined with other algorithms [83–86]. Therefore, we prefer to provide a comparison of the algorithms with the highest order of magnitude of computational complexity, and more detailed algorithm information can be obtained from the table references. In Table 5, N denotes the number of RIS reflecting elements, unless otherwise specified in the referenced literature for heuristic and DRL algorithms where N may also represent population size or network dimensions as defined in the corresponding references.

It can be seen from the table that the computational complexity of the traditional optimization algorithm is higher than that of the heuristic algorithm and the DRL algorithm. This is because most of the traditional optimization algorithms use mathematical methods to iteratively optimize the target variable, the number of antennas in the system, the choice of iteration strategy, and convergence conditions which will affect the computational complexity, and most of them need to be combined with other algorithms. For example, SDR, CCM, and other algorithms are only used to solve the unit modulus constraint problem of RIS phase shift. After the process of relaxation and projection, the optimal solution of the established problem needs to be obtained by AO, BCD, ADMM, and other algorithms. Compared with traditional optimization algorithms, heuristic algorithms have the ability to deal with NP-hard problems with complex and large amounts of calculation. Through the appropriate design of population characteristic parameters (such as fitness value, etc.) and search strategy, the global optimal solution of the problem can be obtained with high probability, and the computational complexity is low. However, it is difficult for heuristic algorithms to change the search strategy and make adjustments in time when facing the dynamically changing channel in HSR scenarios. As mentioned above, DRL-based neural network frameworks are able to continuously acquire information from the

environment and make intelligent decisions. Although the computational complexity of the algorithm is not obvious compared with the heuristic algorithm, the learning and training phase of the model can be executed offline, which can greatly reduce the pressure of the system load and delay.



(**a**) (**b**)

Figure 6. Performance–runtime trade-off of different optimization algorithms: (**a**) information transmission rate versus CPU runtime; (**b**) covert throughput versus train speed.

Figure 6 illustrates the performance of several algorithms discussed in Table 5 from the following two complementary perspectives: (a) the information transmission rate versus CPU run time, and (b) the covert throughput versus train speed. As shown in Figure 6a, CCM, BCD, and similar algorithms can provide a high information transmission rate within a short running time, but their computational complexity is high, and they usually need to be combined with other algorithms when facing multi-constraint problems. The running time of SDR, ROE, and related algorithms is long, making them unsuitable for fast-moving HSR scenarios. GD, APG, MM, and GA exhibit moderate performance in terms of both running time and information transmission rate. Although the DDPG algorithm does not achieve the best performance and its running time is higher than that of CCM, GD, and some other algorithms, the training phase of DRL frameworks can be performed offline. In the ideal case, offline training can almost eliminate the latency introduced by real-time data processing. In addition, DDPG combined with MDP can directly solve the multi-constraint non-convex coupling problem without resorting to other algorithms, which further reduces the computational complexity and time overhead of the algorithm.

Figure 6b compares the impact of train speed variation on the system covert throughput. The covert throughput of the proposed DDPG algorithm and the comparison algorithms all gradually decreases as the train speed increases. However, the proposed DDPG algorithm exhibits relatively stable performance after the train speed exceeds 144 km/h, indicating that it can adapt to high-mobility scenarios with good robustness. In contrast, the covert throughput of the BCD and AO1 algorithms decreases sharply and fluctuates significantly as the train speed increases. The main reason is that the BCD algorithm, when using train position information for beam alignment, does not account for the accumulation of Doppler shift caused by high train speed during operation, which leads to severe train positioning errors and deteriorates algorithm performance. The AO1 algorithm is mainly designed to provide communication services for low-speed and stationary users; when applied to HSR communication scenarios, the rapid user movement, Doppler shift effect, and train penetration loss seriously degrade its performance. In addition, when the train speed is below 252 km/h, the performance of the DDPG algorithm is almost consistent with that of the AO algorithm. As the train speed continues to increase, however, the

disadvantage of traditional mathematical algorithms in dynamic adaptability becomes apparent, and the covert throughput performance drops rapidly. In contrast, DRL can continuously perceive environmental changes and adjust its learning strategy, thereby ensuring the robustness of covert transmission during train operation. Specifically, in the speed range of 252–504 km/h, the covert throughput of DDPG is on average 13.4% higher than that of the AO algorithm, and the total fluctuation amplitude is on average reduced by 28.8%, demonstrating its strong adaptability to fast time-varying channels.

In summary, in the RIS-assisted HSR covert communication system, the number of antennas, delay, robustness, and concealment of the equipment should be comprehensively considered, and the optimization algorithm should be reasonably selected to solve the problem. It is worth noting that the above-mentioned algorithms are not mutually exclusive in practical applications. For example, a DRL framework can generate an initial solution for the RIS phase shifts during the offline training phase, which is then fine-tuned by BCD or MM algorithms. This hybrid architecture combines the global search capability of DRL with the local convergence precision of traditional optimization methods, offering potential advantages in coping with the rapidly time-varying channels in HSR scenarios.

Table 5. Detailed classification and computational complexity of optimization algorithms.

Categories		Name	Computational Complexity
Relaxation algorithms	Traditional algorithms	SDR [55,75–81]	$\mathcal{O}(N^6)$
		ROE [82,83]	$\mathcal{O}(N^3)$
		RP [84,85]	$\mathcal{O}(N^4)$
Manifold algorithms		CCM [55,86–88]	$\leq\mathcal{O}(N^{4.5})$
		RM [55,89]	$\leq\mathcal{O}(N^{4.5})$
Gradient algorithms		GD [90,91]	$\leq\mathcal{O}(N^4)$
		GB [92]	$\leq\mathcal{O}(N^4)$
		APG [93,94]	$\mathcal{O}(N^2)$
Penalized algorithms		PCCP [55,95–97]	$\mathcal{O}(N^{4.5})$
		ADMM [75,98,99]	$\mathcal{O}(N^3)$
		BFP [100,101]	$\mathcal{O}(N^2)$
Iterative algorithms		BCD [102–104]	$\mathcal{O}(N^3)$
		BCA [106,107]	$\mathcal{O}(N^{4.5})$
		MM [16,90,105]	$\mathcal{O}(N^3)$
	Heuristic algorithms	GA [108]	$\mathcal{O}(N^2)$
		PSO [109,110]	$\mathcal{O}(N^2)$
	Deep reinforcement learning algorithms	DDPG [114]	$\leq\mathcal{O}(N^2)$
		CNN [111,115]	$\leq\mathcal{O}(N^2)$
		DQL [112]	$\leq\mathcal{O}(N^2)$

5. Future Directions

In future communication networks with ubiquitous intelligent connectivity of everything, the cross-research of RIS and wireless covert communication will inevitably promote the development of HSR communication systems in a safer and more intelligent direction. The HSR wireless communication network has the characteristics of rapid change in channel conditions, large Doppler shift, frequent handoff, high level of security requirements,

and complex business types. Although the research on covert communication has made rapid progress in recent years, there are still many challenges in HSR scenarios, such as:

(1) Accurate CSI acquisition in high-speed mobile scenarios. Due to the fast time-varying characteristics of the HSR wireless channel, the research under the assumption of perfect CSI or statistical CSI cannot truly reflect the operation scenario of the train. The literature [55] constructed an RIS-assisted HSR channel model by using train prior information and then proposed an effective estimation method for train positioning error, which provided reference for obtaining real-time CSI of HSR scenes. However, the estimation method for train positioning error requires further study and improvement. Therefore, it is still a difficult problem to accurately obtain the real-time CSI of the channel between the high-speed train and the BS.

(2) Improvement of the covert performance evaluation system. Most of the existing studies consider the detection error probability from the perspective of Willie. However, in the actual HSR scene, the location of Willie is difficult to determine due to the real-time detection requirements, which leads to the inability to obtain the CSI. Therefore, it is impossible to accurately measure the covert communication by relying on the existing covert performance indicators. Future research should design more comprehensive concealment evaluation indicators from the perspective of legitimate receivers and transmitters.

(3) Potential problems of RIS deployment in HSR scenarios. RIS-assisted 5G cellular network communication has made great progress in the aspects of industry, university, research, and application (e.g., coverage expansion, signal enhancement, high-frequency communication, three-dimensional positioning, IoT, edge computing, physical layer security, spectrum sensing and sharing, full-duplex communication, multi-cell communication systems, integrated sensing and communications, etc.), but the application in HSR scenarios is still in the stage of theoretical research. In the actual HSR communication network, the size and location of RIS will have a great impact on the system performance. Therefore, in order to ensure that RIS can provide efficient gain for more networks, it is necessary to accelerate the measurement research of RIS in HSR scenarios.

(4) Hybrid RF/optical communication for railway IoT networks. While this paper focuses on RF/mmWave covert communication, future railway networks will likely adopt heterogeneous architectures integrating both wireless and optical technologies. Optical wireless communication (OWC) and fiber-based solutions can provide ultra-high-capacity backhaul links to complement trackside mmWave/RIS access networks [19]. However, the integration of covert communication requirements into such hybrid systems poses new challenges, including the coordination of security mechanisms across different physical layers and the seamless handover between RF and optical links under high-mobility conditions. This direction warrants further investigation.

6. Conclusions

In this paper, we presented a comprehensive overview of covert communication research in HSR IoT networks. We first summarized the primary security threats facing the new generation of railway IoT systems driven by 5G and other digital technologies, introduced the fundamental covert communication model, and reviewed the seminal work on achievable positive covert capacity. Subsequently, we elaborated on the RIS-assisted millimeter-wave MIMO wireless channel model in HSR IoT environments, compared existing Doppler shift compensation schemes, and proposed a covert constraint design method that takes into account the priority levels of HSR services. Furthermore, taking covert throughput maximization as a case study, we analyzed and compared various

optimization algorithms, providing useful insights for addressing the non-convex coupling problems inherent in HSR covert communications. Finally, we discussed several promising directions for future research.

Importantly, this study demonstrates that incorporating service priority into covert constraint design can effectively strike a balance between security and quality of service (QoS) in RIS-assisted HSR communication systems. However, practical deployment still faces significant engineering challenges, particularly in real-time channel state information (CSI) acquisition and the optimal placement and configuration of RIS panels. Looking forward, the integration of a holistic sensing-communication-security framework into HSR scenarios emerges as a particularly promising avenue, wherein environmental sensing data can be leveraged to inform and enhance covert communication decision-making.

Author Contributions: Conceptualization, Z.Z. and M.Y.; methodology, Z.Z.; software, Z.Z.; validation, Z.Z.; formal analysis, J.J.; investigation, Z.Z.; resources, Z.Z.; data curation, Z.Z.; writing—original draft preparation, Z.Z.; writ-ing—review and editing, Z.Z.; visualization, Z.Z.; supervision, Z.Z.; project administration, Z.Z.; funding acquisition, M.Y. and J.J. All authors have read and agreed to the published version of the manuscript.

Funding: This work was supported in part by the Gansu Provincial Department of Education University Teacher Innovation Foundation under Grant 2025B-171, the Youth Foundation of Lanzhou City University under Grant LZCU-QN2025-01, the Jiangxi Provincial Natural Science Foundation (20262BAC200188), Early-Career Young Scientists and Technologists Project of Jiangxi Province (20252BEJ730250), Guidance Plan Project for Industrial Development of Jingdezhen (2025GY019).

Data Availability Statement: The original contributions presented in this study are included in the article. Further inquiries can be directed to the corresponding author.

Conflicts of Interest: The authors declare no conflicts of interest.

References

1. Pang, W.; Zhang, Y. Optimization of Sum-Rate for Downlink Transmission in Hybrid RIS-Assisted MISO Systems. *Telecom* **2026**, *7*, 26. [CrossRef]
2. Yang, M.; Xie, J.; Ban, Y.; Yang, M.; Xie, J.; Ban, Y.; Gao, Y.; Ai, B.; Li, C. Reconfigurable Intelligent Surface-aided High-Speed Railway Integrated Sensing and Communications Based on Deep Reinforcement Learning. *IEEE Trans. Wirel. commun.* **2026**, *25*, 16272–16287. [CrossRef]
3. Li, P.; Wu, H.; Liu, J. Overview of security technologies and strategies for intelligent railway 5G. *Comput Sci.* **2024**, *51*, 1–11.
4. Wei, Z.; Liu, F.; Masouros, C.; Su, N.; Petropulu, A.P. Toward multi-functional 6G wireless networks: Integrating sensing, communication, and security. *IEEE Commun. Mag.* **2022**, *60*, 65–71. [CrossRef]
5. Li, C.; Sun, S.; Zhang, Z.; Li, C.; Sun, S.; Zhang, Z.; Ai, B.; Wu, H.; Xie, J. IRS-Assisted High-Speed Railway Secure Communications: Deep Learning for Joint Beamforming. *IEEE Trans. Intelli. Transpor. Syst.* **2026**, *27*, 4645–4655. [CrossRef]
6. Zhang, Z.; Li, C.; Wu, H.; Zepeng, Z.; Cuiran, L.; Hao, W.; Jianli, X. Reconfigurable Intelligent Surface-aided MIMO covert communications in High-Speed Railway scenario. *China Commun.* **2024**, *22*, 109–123. [CrossRef]
7. Li, P.; Niu, Y.; Wu, H.; Han, Z.; Ai, B.; Wang, N.; Li, P.; Niu, Y.; Wu, H.; Han, Z.; et al. RIS-assisted scheduling for high-speed railway secure communications. *IEEE Trans. Veh. Technol.* **2022**, *72*, 3488–3501. [CrossRef]
8. Chen, W.; Luo, J.; Wang, F. Survey of capacity limits and implementation techniques in wireless covert communication. *J. Commun.* **2022**, *43*, 203–218.
9. Li, C.; Luan, J.; Zhang, Z.; Ai, B.; Wu, H.; Xie, J. Deep Reinforcement Learning-Based Joint Optimization for Physical Layer Security in IRS-Assisted High-Speed Railway Networks. *IEEE Trans. Net. Sci. Eng.* **2025**, *13*, 3846–3861. [CrossRef]
10. Zhang, Z.; Liu, Y.; Wang, Z.; Mu, X.; Chen, J. Physical layer security in near-field communications. *IEEE Trans. Veh. Technol.* **2024**, *73*, 10761–10766. [CrossRef]
11. Chen, X.; An, J.; Xiong, Z.; Xing, C.; Zhao, N.; Yu, F.R.; Nallanathan, A. Covert communications: A comprehensive survey. *IEEE Commun. Surv. Tutor.* **2023**, *25*, 1173–1198. [CrossRef]
12. Li, L.; Zhao, H.; Liu, C.; Li, L.; Cui, T.J. Intelligent metasurfaces: Control, communication and computing. *eLight* **2022**, *2*, 7. [CrossRef]

13. Chen, F.; Zhang, R. Research on IoV resource allocation algorithm assisted by reconfigurable intelligent surface. *J. Commun.* **2023**, *44*, 70–78.
14. Ao, S.; Niu, Y.; Han, Z.; Ai, B.; Zhong, Z.; Wang, N.; Qiao, Y. Resource allocation for RIS assisted device-to-device communications in heterogeneous cellular networks. *IEEE Trans. Veh. Technol.* **2023**, *72*, 11741–11755. [CrossRef]
15. Pan, C.; Zhou, G.; Zhi, K.; Hong, S.; Wu, T.; Pan, Y.; Ren, H.; Di Renzo, M.; Swindlehurst, A.L.; Zhang, R.; et al. An overview of signal processing techniques for RIS/IRS-aided wireless systems. *IEEE J. Sel. Top. Signal Process.* **2022**, *16*, 883–917. [CrossRef]
16. Zheng, B.; You, C.; Mei, W.; Zhang, R. A survey on channel estimation and practical passive beamforming design for intelligent reflecting surface aided wireless communications. *IEEE Commun. Surv. Tutor.* **2022**, *24*, 1035–1071. [CrossRef]
17. Wang, K.; Lam, C.; Ng, B. Positioning information based high-speed communications with multiple RIS: Doppler mitigation and hardware impairments. *Appl. Sci.* **2022**, *12*, 7076. [CrossRef]
18. Basar, E. Reconfigurable intelligent surfaces for Doppler effect and multipath fading mitigation. *Front. Comm. Net.* **2021**, *2*, 672–680. [CrossRef]
19. Alhalabi, M.; Taşpınar, N.; Wadi, M.; Salemdeeb, M. Performance analysis of a low-cost directly modulated OFDM-based optical wireless communication systems. *Wirel. Pers. Commun.* **2026**, *146*, 1415–1441. [CrossRef]
20. Bash, B.; Goeckel, D.; Towsley, D. Limits of reliable communication with low probability of detection on AWGN channels. *IEEE J. Sel. Areas Comm.* **2013**, *31*, 1921–1930. [CrossRef]
21. Wang, C.; Li, Z.; Shi, J.; Ng, D.W.K. Intelligent reflecting surface assisted multi-antenna covert communications: Joint active and passive beamforming optimization. *IEEE Trans. Commun.* **2021**, *69*, 3984–4000. [CrossRef]
22. Zhou, X.; Yan, S.; Shu, F.; Chen, R.; Li, J. UAV-enabled covert wireless data collection. *IEEE J. Sel. Areas Comm.* **2021**, *39*, 3348–3362. [CrossRef]
23. Wang, M.; Xia, B.; Yao, Y.; Chen, Z.; Wang, J. Fundamental limit among covertness, reliability, latency and throughput for IRS enabled short-packet communications. *IEEE Trans. Wirel. Commun.* **2024**, *23*, 3886–3900. [CrossRef]
24. He, B.; Yan, S.; Zhou, X.; Lau, V.K.N. On covert communication with noise uncertainty. *IEEE Commun. Lett.* **2017**, *21*, 941–944. [CrossRef]
25. Tao, L.; Yang, W.; Yan, S.; Wu, D.; Guan, X.; Chen, D. Covert communication in downlink NOMA systems with random transmit power. *IEEE Wirel. Commun. Lett.* **2020**, *9*, 2000–2004. [CrossRef]
26. Sun, R.; Yang, B.; Ma, S.; Shen, Y.; Jiang, X. Covert rate maximization in wireless full-duplex relaying systems with power control. *IEEE Trans. Commun.* **2021**, *69*, 6198–6212. [CrossRef]
27. Yang, L.; Yang, W.; Xu, S.; Tang, L.; He, Z. Achieving covert wireless communications using a full-duplex multi-antenna receiver. In *2019 IEEE 5th International Conference on Computer and Communications (ICCC)*; IEEE: Piscataway, NJ, USA, 2019; pp. 912–916.
28. Lin, Y.; Jin, L.; Zhou, Y.; Lou, Y. Performance analysis of covert wireless communication based on beam forming with noise uncertainty. *J. Commun.* **2020**, *41*, 49–58.
29. Lee, S.; Wang, L.; Khisti, A.; Wornell, G.W. Covert communication with channel-state information at the transmitter. *IEEE Trans. Inf. Forensics Secur.* **2018**, *13*, 2310–2319. [CrossRef]
30. Sobers, T.; Bash, B.; Guha, S.; Towsley, D.; Goeckel, D. Covert communication in the presence of an uninformed jammer. *IEEE Trans. Wirel. Commun.* **2017**, *16*, 6193–6206. [CrossRef]
31. Wang, J.; Tang, W.; Zhu, Q.; Li, X.; Rao, H.; Li, S. Covert communication with the help of relay and channel uncertainty. *IEEE Wirel. Commun. Lett.* **2018**, *8*, 317–320. [CrossRef]
32. Lin, Y.; Jin, L.; Huang, K.; Sun, X.; Wang, F. Multiantenna joint covert communication system with finite blocklength. *IEEE Syst. J.* **2022**, *17*, 1170–1180. [CrossRef]
33. Lin, M.; Wang, W. Multi-carrier wireless covert communication with delay constraint. *IEEE Trans. Veh. Technol.* **2022**, *72*, 5350–5355. [CrossRef]
34. Li, K.; Sobers, T.V.; Towsley, D.; Goeckel, D. Covert communication in continuous-time systems in the presence of a jammer. *IEEE Trans. Wirel. Commun.* **2022**, *21*, 4883–4897. [CrossRef]
35. Soltani, R.; Goeckel, D.; Towsley, D.; Bash, B.A.; Guha, S. Covert wireless communication with artificial noise generation. *IEEE Trans. Wirel. Commun.* **2018**, *17*, 7252–7267. [CrossRef]
36. Liu, Z.; Liu, J.; Zeng, Y.; Ma, J. Covert wireless communication in IoT network: From AWGN channel to THz band. *IEEE Internet Things J.* **2020**, *7*, 3378–3388. [CrossRef]
37. Sheikholeslami, A.; Ghaderi, M.; Towsley, D.; Bash, B.A.; Guha, S.; Goeckel, D. Multi-hop routing in covert wireless networks. *IEEE Trans. Wirel. Commun.* **2018**, *17*, 3656–3669. [CrossRef]
38. Ma, S.; Zhang, Y.; Li, H.; Lu, S.; Al-Dhahir, N.; Zhang, S.; Li, S. Robust beamforming design for covert communications. *IEEE Trans. Inf. Forensics Secur.* **2021**, *16*, 3026–3038. [CrossRef]
39. Lira, W.P.; Alves, R.; Costa, J.M.; Pessin, G.; Galvão, L.; Cardoso, A.C.; de Souza, C.R. A Visual-Analytics System for Railway Safety Management. *IEEE Comput. Graph. Appl.* **2014**, *34*, 52–57. [CrossRef] [PubMed]

40. Wang, M.; Yang, W.; Lu, X.; Hu, C.; Liu, B.; Lv, X. Channel inversion power control aided covert communications in uplink NOMA systems. *IEEE Wirel. Commun. Lett.* **2022**, *11*, 871–875. [CrossRef]
41. Shmuel, O.; Cohen, A.; Gurewitz, O. Multi-antenna jamming in covert communication. *IEEE Trans. Commun.* **2021**, *69*, 4644–4658. [CrossRef]
42. Zheng, T.; Wang, H.; Ng, D.; Yuan, J. Multi-antenna covert communications in random wireless networks. *IEEE Trans. Wirel. Commun.* **2019**, *18*, 1974–1987. [CrossRef]
43. Chen, X.; Sun, W.; Xing, C.; Zhao, N.; Chen, Y.; Yu, F.R.; Nallanathan, A. Multi-antenna covert communication via full-duplex jamming against a warden with uncertain locations. *IEEE Trans. Wirel. Commun.* **2021**, *20*, 5467–5480. [CrossRef]
44. Xu, D.; Zhu, H. Proactive eavesdropping of wireless powered suspicious interference networks. *Sci. China Inf. Sci.* **2021**, *64*, 229–305. [CrossRef]
45. Yan, S.; He, B.; Zhou, X.; Cong, Y.; Swindlehurst, A.L. Delay-intolerant covert communications with either fixed or random transmit power. *IEEE Trans. Inf. Forensics Secur.* **2019**, *14*, 129–140. [CrossRef]
46. He, B.; Yan, S.; Zhou, X.; Jafarkhani, H. Covert wireless communication with a Poisson field of interferers. *IEEE Trans. Wirel. Commun.* **2018**, *17*, 6005–6017. [CrossRef]
47. Bendary, A.; Abdelzaiz, A.; Koksal, C. Achieving positive covert capacity over MIMO AWGN channels. *IEEE J. Sel. Areas Inf. Theory* **2021**, *2*, 149–162. [CrossRef]
48. Shahzad, K.; Zhou, X.; Yan, S. Covert wireless communication in presence of a Multi-Antenna adversary and delay constraints. *IEEE Trans. Veh. Technol.* **2019**, *68*, 12432–12436. [CrossRef]
49. Lin, J.; Jin, L.; Huang, K.; Han, Q. Threat region development of covert wireless communication based on 3D beamforming. *Sci. Sin.* **2021**, *51*, 1360–1374. [CrossRef]
50. Yu, X.; Luo, Y.; Chen, W. Covert communication with beamforming over MISO channels in the finite blocklength regime. *Sci. China Inf. Sci.* **2021**, *64*, 183–197. [CrossRef]
51. Chen, X.; Zheng, T.; Dong, L.; Lin, M.; Yuan, J. Enhancing MIMO covert communications via intelligent reflecting surface. *IEEE Wirel. Commun. Lett.* **2021**, *11*, 33–37. [CrossRef]
52. Faragallah, O.; Elsayed, H.; Emashed, M. High mobility transmission system under intelligent reflecting surface. *Trans. Emerg. Telecommun. Technol.* **2022**, *33*, 4495–4513. [CrossRef]
53. Kim, J.; Hosseinalipour, S.; Kim, T.; Love, D.J.; Brinton, C.G. Multi-IRS Assisted Multi-cell Uplink MIMO Communications Under Imperfect CSI: A Deep Reinforcement Learning Approach. In *2021 IEEE International Conference on Communications Workshops (ICC Workshops)*; IEEE: Piscataway, NJ, USA, 2021; pp. 1–7.
54. Guo, C.; Cui, Y.; Yang, F.; Ding, L. Outage probability analysis and minimization in intelligent reflecting surface-assisted MISO systems. *IEEE Commun. Lett.* **2020**, *24*, 1563–1567. [CrossRef]
55. Zhang, Z.; Li, C.; Wu, H.; Xie, J.; Xu, Q. Robust beamforming algorithm for RIS-MIMO system based on train prior information. *J. Commun.* **2024**, *45*, 29–43.
56. Mao, Z.; Peng, M.; Liu, X. Channel estimation for reconfigurable intelligent surface assisted wireless communication systems in mobility scenarios. *China Commun.* **2021**, *18*, 29–38. [CrossRef]
57. Sun, S.; Yan, H. Channel estimation for reconfigurable intelligent surface-assisted wireless communications considering Doppler effect. *IEEE Wirel. Commun. Lett.* **2020**, *10*, 790–794. [CrossRef]
58. Huang, Z.; Zheng, B.; Zhang, R. Transforming fading channel from fast to slow: Intelligent refracting surface aided high mobility communication. *IEEE Trans. Wirel. Commun.* **2021**, *21*, 4989–5003. [CrossRef]
59. Xu, W.; An, J.; Xu, Y.; Huang, C.; Gan, L.; Yuen, C. Time-varying channel prediction for RIS-assisted MU-MISO networks via deep learning. *IEEE Trans. Cogn. Commun. Netw.* **2022**, *8*, 1802–1815. [CrossRef]
60. Zhang, C.; Wang, G.; Jia, M.; He, R.; Zhou, L.; Ai, B. Doppler shift estimation for millimeter-wave communication systems on high-speed railways. *IEEE Access* **2018**, *7*, 40454–40462. [CrossRef]
61. Li, C.; Lu, Y.; Xie, J.; Zhang, Z. An energy-efficient optimization method for high-speed rail communication systems assisted by intelligent reflecting surfaces (IRS). *Appl. Sci.* **2023**, *13*, 9401. [CrossRef]
62. Wu, G.; Li, F.; Jiang, H. Analysis of multipath fading and Doppler effect with multiple reconfigurable intelligent surfaces in mobile wireless networks. *Wirel. Commun. Mob. Comput.* **2022**, *2022*, 5751–5762. [CrossRef]
63. Hu, X.; Zhong, C.; Alouini, M.S.; Zhang, Z. Robust design for IRS aided communication systems with user location uncertainty. *IEEE Wirel. Commun. Lett.* **2020**, *10*, 63–67. [CrossRef]
64. Li, C.; Zhang, Z.; Xie, J. Handover Algorithm Based on LSTM Dynamic Beamforming for High-speed Train. *J. China Railw. Soc.* **2023**, *45*, 78–86.
65. Wang, C.; Li, Z.; Zheng, T.; Ng, D.W.K.; Al-Dhahir, N. Intelligent reflecting surface-aided full-duplex covert communications: Information freshness optimization. *IEEE Trans. Wirel. Commun.* **2022**, *22*, 3246–3263. [CrossRef]
66. Zhou, X.; Yu, H.; Peng, X. Wireless covert communications based on intelligent reflecting surface aided and artificial noise enhanced. *J. Electron. Z. Inf. Technol.* **2022**, *44*, 2392–2399.

67. Deng, D.; Li, X.; Dang, S.; Gursoy, M.C.; Nallanathan, A. Covert communications in intelligent reflecting surface-assisted two-way relaying networks. *IEEE Trans. Veh. Technol.* **2022**, *71*, 12380–12385. [CrossRef]
68. Li, C.; Guo, Q.; Yan, X. Research on service quality assurance of intelligent dispatching communication service based on 5G-R. *Railw. Signal. Commun.* **2022**, *58*, 17–21+36.
69. Zhao, F.; Wang, Y.; Jia, L.; Xia, W. High-Speed Railway intelligent operation business improvement demand and key technologies for implementation. *China Railw.* **2024**, 134–144.
70. Ma, S.; Zhang, Y.; Li, H.; Sun, J.; Shi, J.; Zhang, H.; Shen, C.; Li, S. Covert beamforming design for intelligent-reflecting-surface-assisted IoT networks. *IEEE Internet Things J.* **2021**, *9*, 5489–5501. [CrossRef]
71. Yan, S.; Cong, Y.; Hanly, S.; Zhou, X. Gaussian signaling for covert communications. *IEEE Trans. Wirel. Commun.* **2019**, *18*, 3542–3553. [CrossRef]
72. Polyanskiy, Y.; Vincent, H.; Verdu, S. Channel coding rate in the finite block length regime. *IEEE Trans. Inf. Theory* **2010**, *56*, 2307–2359. [CrossRef]
73. Jiang, H.; You, L.; Wang, J.; Wang, W.; Gao, X. Hybrid RIS and DMA assisted multiuser MIMO uplink transmission with electromagnetic exposure constraints. *IEEE J. Sel. Top. Signal Process.* **2022**, *16*, 1055–1069. [CrossRef]
74. Guo, H.; Liang, Y.; Chen, J.; Larsson, E.G. Weighted Sum-rate Maximization for Intelligent Reflecting Surface Enhanced Wireless Networks. In *2019 IEEE Global Communications Conference (GLOBECOM)*; IEEE: Piscataway, NJ, USA, 2019; pp. 1–6.
75. Wu, Q.; Zhang, R. Intelligent reflecting surface enhanced wireless network via joint active and passive beamforming. *IEEE Trans. Wirel. Commun.* **2019**, *18*, 5394–5409. [CrossRef]
76. Cui, M.; Zhang, G.; Zhang, R. Secure wireless communication via intelligent reflecting surface. *IEEE Wirel. Commun. Lett.* **2019**, *8*, 1410–1414. [CrossRef]
77. Chu, Z.; Hao, W.; Xiao, P.; Shi, J. Intelligent reflecting surface aided multi-antenna secure transmission. *IEEE Wirel. Commun. Lett.* **2019**, *9*, 108–112. [CrossRef]
78. Wang, P.; Fang, J.; Yuan, X.; Chen, Z.; Li, H. Intelligent reflecting surface-assisted millimeter-wave communications: Joint active and passive precoding design. *IEEE Trans. Veh. Technol.* **2020**, *69*, 14960–14973. [CrossRef]
79. Yang, G.; Xu, X.; Liang, Y.; Renzo, M.D. Reconfigurable intelligent surface-assisted non-orthogonal multiple access. *IEEE Trans. Wirel. Commun.* **2021**, *20*, 3137–3151. [CrossRef]
80. Zhou, G.; Pan, C.; Ren, H.; Wang, K.; Peng, Z. Secure wireless communication in RIS-aided MISO system with hardware impairments. *IEEE Wirel. Commun. Lett.* **2021**, *10*, 1309–1313. [CrossRef]
81. Zeng, M.; Li, X.; Li, G.; Hao, W.; Dobre, O.A. Sum rate maximization for IRS-assisted uplink NOMA. *IEEE Commun. Lett.* **2020**, *25*, 234–238. [CrossRef]
82. Fu, M.; Zhou, Y.; Shi, Y. Intelligent reflecting surface for downlink non-orthogonal multiple access networks. In *Intelligent Reflecting Surface for Downlink Non-Orthogonal Multiple Access Networks*; IEEE: Piscataway, NJ, USA, 2019; pp. 1–6.
83. Hu, X.; Masouros, C.; Wong, K. Reconfigurable intelligent surface aided mobile edge computing: From optimization-based to location-only learning-based solutions. *IEEE Trans. Commun.* **2021**, *69*, 3709–3725. [CrossRef]
84. Chen, J.; Liang, Y.; Pei, Y.; Guo, H. Intelligent reflecting surface: A programmable wireless environment for physical layer security. *IEEE Access* **2019**, *7*, 82599–82612. [CrossRef]
85. Zhou, G.; Pan, C.; Ren, H.; Wang, K.; Elkashlan, M.; Renzo, M.D. Stochastic learning-based robust beamforming design for RIS-aided millimeter-wave systems in the presence of random blockages. *IEEE Trans. Veh. Technol.* **2021**, *70*, 1057–1061. [CrossRef]
86. Wang, P.; Fang, J.; Dai, L.; Li, H. Joint transceiver and large intelligent surface design for massive MIMO mmWave systems. *IEEE Trans. Wirel. Commun.* **2020**, *20*, 1052–1064. [CrossRef]
87. Pan, C.; Ren, H.; Wang, K.; Xu, W.; Elkashlan, M.; Nallanathan, A.; Hanzo, L. Multicell MIMO communications relying on intelligent reflecting surfaces. *IEEE Trans. Wirel. Commun.* **2020**, *19*, 5218–5233. [CrossRef]
88. Guo, H.; Liang, Y.; Chen, J.; Larsson, E.G. Weighted sum-rate maximization for reconfigurable intelligent surface aided wireless networks. *IEEE Trans. Wirel. Commun.* **2020**, *19*, 3064–3076. [CrossRef]
89. Tang, C.; Rong, X.; Jian, J.; Xing, S. A hybrid Riemannian conjugate gradient method for nonconvex optimization problems. *J. Appl. Math. Comput.* **2023**, *69*, 823–852. [CrossRef]
90. Huang, C.; Zappone, A.; Alexandropoulos, G.; Debbah, M.; Yuen, C. Reconfigurable intelligent surfaces for energy efficiency in wireless communication. *IEEE Trans. Wirel. Commun.* **2019**, *18*, 4157–4170. [CrossRef]
91. Perović, N.; Tran, L.; Di, R.; Flanagan, M.F. Achievable rate optimization for MIMO systems with reconfigurable intelligent surfaces. *IEEE Trans. Wirel. Commun.* **2021**, *20*, 3865–3882. [CrossRef]
92. Zhi, K.; Pan, C.; Ren, H.; Wang, K.; Elkashlan, M.; Renzo, M.D.; Schober, R.; Poor, H.V.; Wang, J.; Hanzo, L. Two-timescale design for reconfigurable intelligent surface-aided massive MIMO systems with imperfect CSI. *IEEE Trans. Inf. Theory* **2022**, *69*, 3001–3033. [CrossRef]
93. Shao, M.; Li, Q.; Ma, W. Minimum symbol-error probability symbol-level precoding with intelligent reflecting surface. *IEEE Wirel. Commun. Lett.* **2020**, *9*, 1601–1605. [CrossRef]

94. Perović, N.; Tran, L.; Di, R.; Flanagan, M.F. Optimization of RIS-aided MIMO systems via the cutoff rate. *IEEE Wirel. Commun. Lett.* **2021**, *10*, 1692–1696. [CrossRef]
95. Zhou, G.; Pan, C.; Ren, H.; Wang, K.; Nallanathan, A. A framework of robust transmission design for IRS-aided MISO communications with imperfect cascaded channels. *IEEE Trans. Signal Process.* **2020**, *68*, 5092–5106. [CrossRef]
96. Zhang, L.; Pan, C.; Wang, Y.; Ren, H.; Wang, K. Robust beamforming design for intelligent reflecting surface aided cognitive radio systems with imperfect cascaded CSI. *IEEE Trans. Cogn. Commun. Netw.* **2021**, *8*, 186–201. [CrossRef]
97. Chen, Y.; Wang, Y.; Jiao, L. Robust transmission for reconfigurable intelligent surface aided millimeter-wave vehicular communications with statistical CSI. *IEEE Trans. Wirel. Commun.* **2021**, *21*, 928–944. [CrossRef]
98. Huang, K.; Wang, H. Passive beamforming for IRS aided wireless networks. *IEEE Wirel. Commun. Lett.* **2020**, *9*, 2035–2039. [CrossRef]
99. Yang, H.; Yuan, X.; Fang, J.; Liang, Y.C. Reconfigurable intelligent surface aided constant-envelope wireless power transfer. *IEEE Trans. Signal Process.* **2021**, *69*, 1347–1361. [CrossRef]
100. Ye, J.; Guo, S.; Alouini, M. Joint reflecting and precoding designs for SER minimization in reconfigurable intelligent surfaces assisted MIMO systems. *IEEE Trans. Wirel. Commun.* **2020**, *19*, 5561–5574. [CrossRef]
101. Hu, X.; Zhong, C.; Zhang, Z. Angle-domain intelligent reflecting surface systems: Design and analysis. *IEEE Trans. Commun.* **2021**, *69*, 4202–4215. [CrossRef]
102. Yu, X.; Xu, D.; Schober, R. Enabling Secure Wireless Communications via Intelligent Reflecting Surfaces. In *2019 IEEE Global Communications Conference (GLOBECOM)*; IEEE: Piscataway, NJ, USA, 2019; pp. 1–6.
103. Zeng, M.; Bedeer, E.; Dobre, O.; Fortier, P.; Pham, Q.-V.; Hao, W. Energy-efficient resource allocation for IRS-assisted multi-antenna uplink systems. *IEEE Wirel. Commun. Lett.* **2021**, *10*, 1261–1265. [CrossRef]
104. Wu, Q.; Zhang, R. Joint active and passive beamforming optimization for intelligent reflecting surface assisted SWIPT under QoS constraints. *IEEE J. Sel. Areas Comm.* **2020**, *38*, 1735–1748. [CrossRef]
105. Peng, Z.; Zhang, Z.; Pan, C.; Li, L.; Swindlehurst, A.L. Multiuser full-duplex two-way communications via intelligent reflecting surface. *IEEE Trans. Signal Process.* **2021**, *69*, 837–851. [CrossRef]
106. González, P.; Fresnedo, Ó.; Castedo, L. A rank-constrained coordinate ascent approach to hybrid precoding for the downlink of wideband massive MIMO systems. *IEEE Trans. Veh. Technol.* **2023**, *72*, 15953–15966. [CrossRef]
107. Zhang, D.; Wu, Q.; Cui, M.; Zhang, G.; Niyato, D. Throughput maximization for IRS-assisted wireless powered hybrid NOMA and TDMA. *IEEE Wirel. Commun. Lett.* **2021**, *10*, 1944–1948. [CrossRef]
108. Zhi, K.; Pan, C.; Ren, H.; Wang, K. Power scaling law analysis and phase shift optimization of RIS-aided massive MIMO systems with statistical CSI. *IEEE Trans. Commun.* **2022**, *70*, 3558–3574. [CrossRef]
109. Tan, F.; Xu, X.; Chen, H.; Li, S. Energy-efficient beamforming optimization for MISO communication based on reconfigurable intelligent surface. *Phys. Commun.* **2023**, *4*, 101–116. [CrossRef]
110. Dai, J.; Wang, Y.; Pan, C.; Zhi, K.; Ren, H.; Wang, K. Reconfigurable intelligent surface aided massive MIMO systems with low-resolution DACs. *IEEE Commun. Lett.* **2021**, *25*, 3124–3128. [CrossRef]
111. Yang, H.; Xiong, Z.; Zhao, J.; Niyato, D.; Xiao, L.; Wu, Q. Deep reinforcement learning based Intelligent Reflecting Surface for secure wireless communications. *IEEE Trans. Wirel. Commun.* **2021**, *20*, 375–388. [CrossRef]
112. Huang, C.; Mo, R.; Yuen, C. Reconfigurable intelligent surface assisted multiuser MISO systems exploiting deep reinforcement learning. *IEEE J. Sel. Areas Comm.* **2020**, *38*, 1839–1850. [CrossRef]
113. Feng, K.; Wang, Q.; Li, X.; Wen, C.-K. Deep reinforcement learning based intelligent reflecting surface optimization for MISO communication systems. *IEEE Wirel. Commun. Lett.* **2020**, *9*, 745–749. [CrossRef]
114. Xu, J.; Ai, B.; Quek, T. Toward interference suppression: RIS-aided high-speed railway networks via deep reinforcement learning. *IEEE Trans. Wirel. Commun.* **2022**, *22*, 4188–4201. [CrossRef]
115. Shen, W.; Qin, Z.; Nallanathan, A. Deep learning for super-resolution channel estimation in reconfigurable intelligent surface aided systems. *IEEE Trans. Commun.* **2023**, *71*, 1491–1503. [CrossRef]

Disclaimer/Publisher's Note: The statements, opinions and data contained in all publications are solely those of the individual author(s) and contributor(s) and not of MDPI and/or the editor(s). MDPI and/or the editor(s) disclaim responsibility for any injury to people or property resulting from any ideas, methods, instructions or products referred to in the content.